Journal of Materials Chemistry A

COMMUNICATION

View Article Online
View Journal | View Issue

Rational design of hybrid dye-sensitized solar cells composed of double-layered photoanodes with enhanced power conversion efficiency†

Cite this: *J. Mater. Chem. A*, 2014, **2**, 11035

Received 4th May 2014
Accepted 8th May 2014

DOI: 10.1039/c4ta02232g

www.rsc.org/MaterialsA

Xiaodan Zhang,[ab] Wenming Liao,[a] Wei Mu,[bc] Dajiang Zheng,[a] Yusheng Zhou,[a] Bailiang Xue,[b] Wei Liu,[c] Zhiqun Lin[a] and Yulin Deng*[bc]

A uniquely structured dye-sensitized solar cell was fabricated by assembling two photoanodes and one counter electrode in a single compartment. The two photoanodes have complementary roles in absorbing solar light at different wavelengths. The power conversion efficiency of the hybrid cell can reach 6.6%, which is significantly higher than that of the single cell. The rational design of the hybrid cell does not need an interconnecting layer as that is used in conventional tandem solar cells, leading to higher power conversion efficiency.

Dye-sensitized solar cells (DSSCs) have been studied extensively because of their low cost compared to Si based solar cells.[1] Great effort has been made to improve their power conversion efficiency to sharpen their competitive edge over Si based solar cells.[2–12] Different methods have been adopted to realize better power conversion efficiency. One attempt is to develop a high-efficiency dye which can absorb as much light as possible in intensity and over a broader solar spectrum.[13,14] However, it is difficult to achieve high photoelectric conversion and low charge recombination at the same time for high-efficiency dye design. Another method is to use simultaneous or stepwise co-sensitization of multiple dyes for cell fabrication.[15–18] Co-sensitization compensates the disadvantages of absorption limitation of a single dye and broadens the solar wavelength absorption range. However, in the simultaneously co-sensitized DSSCs,[19,20] there is an absorption competition between different dyes, and possible negative interaction between these dyes also occurs. As a result, the total light conversion is only slightly improved or even lowered compared to a single DSSC. While in the case of stepwise co-sensitization of DSSCs,[21–25] two or more different dye-sensitized semiconductor layers (usually TiO_2 or ZnO) will be coated stepwise on a conductive substrate. Clearly, with the increase of the semiconductor thickness, difficulties will be encountered for successful injection of electrons into the conductive substrate.

Tandem or hybrid solar cells are also used to harvest more solar energy.[26,27] Generally, these cells were fabricated by vertically stacking two or more subcells connected by an interconnecting layer. Tandem/hybrid cells have the advantages of broadening the absorption spectrum and avoiding negative interaction among dyes. Nelles *et al.* designed tandem DSSCs with red dye and black dye in the upper and lower compartments, respectively.[28] However, in their design, the incident light needs to pass through multiple electrodes, including two working electrodes and one semitransparent counter electrode, to reach the lower dye. This would reduce the light absorption of the bottom cell. Murayama and Mori designed a face to face tandem cell structure with two dye-sensitized TiO_2 at each side as working electrodes and a platinum mesh in the middle as the counter electrode.[29] A homogeneous DSSC (N3 dye-sensitized TiO_2) and a heterogeneous DSSC (N3 dye and black dye-sensitized TiO_2) were tested in this design, with power conversion efficiency being 1.8% and 3.9%, respectively. Likewise, the middle counter electrode, or called the interconnecting layer, would block the part of solar energy, leading to low efficiency. Yamaguchi *et al.* fabricated tandem dye-sensitized solar cells on a glass rod, in which two different dye-sensitized TiO_2 layers were assembled along the glass rod.[30] These tandem cells showed a low power conversion of 1.33%. The reason for the low efficiency was that almost all of the light passed through the glass rods directly without being absorbed. Only a small portion of the light contacting the interface between the glass rod and the TiO_2/dye layer was used for photoconversion.

Although tandem solar cells commonly have higher efficiency than a single solar cell, there are many challenges in order to further improve their performance. For example, to connect two or more subcells in a series, interconnecting layers

[a]*School of Materials Science and Engineering, Georgia Institute of Technology, Atlanta, GA 30318, USA*

[b]*Institute of Paper Science & Technology, Georgia Institute of Technology, 500 10th Street, NW, Atlanta, GA 30318, USA. E-mail: yulin.deng@ipst.gatech.edu; Tel: +1 404 894 5759*

[c]*School of Chemical & Biomolecular Engineering, Georgia Institute of Technology, Atlanta, GA 30318, USA*

† Electronic supplementary information (ESI) available. See DOI: 10.1039/c4ta02232g

have to be used. Ideally, the interconnecting layers should have sufficient conductivity, high transparency, good uniformity and high chemical stability. Their energy levels should also match with those of donor/acceptor molecules in the active layer. Unfortunately, such ideal interconnecting layers have not been reported. Besides, compared to solid polymer tandem solar cells, the liquid electrolyte based dye sensitized tandem solar cells are more difficult to fabricate due to the leakage of the electrolyte.

Herein, we report a uniquely structured dye-sensitized solar cell that has double-layered photoanodes with two different dyes, but only one counter cathode as shown in Fig. 1. Different from traditional DSSCs, a second photoanode layer is inserted between the traditional anode (with N719 sensitized TiO_2 nanoparticles) and the platinum cathode in our novel design. This second photoanode layer is made of a porous and electrical conducting Ti/Ni mesh with a thin layer of dye-sensitized TiO_2 nanoparticles coated on it. The two photoanodes containing different dyes are assembled face-to-face and connected in a parallel mode as co-anodes. Since the second layer is supported by a porous Ti/Ni mesh, the electrolyte can easily diffuse through this layer to reach the cathode. Because of the two different dye-sensitized TiO_2 layers, such rationally designed hybrid solar cells can absorb more light over a broader wavelength region.

Our double-layered DSSCs are different from conventional tandem solar cells. In our design, there is only one cathode but two parallel connected photoanodes coated with different dyes. The hybrid cells designed in this study allow the incident light to directly reach the second photoanode after passing through the first one, which can reduce the loss of solar energy and internal resistance. More importantly, no interconnecting electrode is needed, which overcomes the bottleneck in fabricating tandem cells. Furthermore, the single-compartment design renders the cells to be more compact and of lower internal resistance. For our hybrid DSSCs, two photoanodes could be separately prepared, thereby eliminating the issues encountered by co-sensitized solar cells.

Fig. 1 shows a schematic diagram of the structure of hybrid solar cells. The top photoanode is made of N719-sensitized TiO_2 on ITO glass. The second photoanode is composed of N749-sensitized TiO_2 on the substrate of the porous Ti/Ni mesh (*i.e.*, 500 nm Ti was sputtered on the Ni mesh). The whole cell compartment is filled with electrolyte solution. The two dyes, N719 and N749, compensate the light absorption range so the solar cell efficiency can be substantially improved. The electrons in the highest occupied molecular orbital (HOMO) of N719 and N749 are excited and injected into TiO_2 nanoparticles and then transport to the ITO and Ti/Ni mesh, respectively. The redox couple in the electrolyte will receive the electrons at the counter electrode and reduce the dye molecules back to their original states. The photo of the hybrid cell is shown in Fig. 1(b).

The SEM images of the Ti/Ni mesh are shown in Fig. 2(a). Clearly, the Ti/Ni mesh is made up of interconnected holes with diameters in the range of 100–250 μm. The porous nature of the Ti/Ni mesh is an essential prerequisite for the electrolyte to penetrate through the whole space in the solar cell compartment. Fig. 2(b) shows the morphology of the TiO_2 nanoparticle (NP) thin film coated on the Ti/Ni mesh. The TiO_2 NP thin film appears to have some cracks, which are beneficial for the electrolyte to flow through. Fig. 2(c) shows the SEM image of the TiO_2 NP. It can be seen that the diameters of the TiO_2 NP range from 20 to 40 nm. Nano-sized pores can be seen among TiO_2 nanoparticles. These nano-sized pores can provide passways for the diffusion of the electrolyte and the adsorption of dye molecules.

Fig. 3 shows the X-ray diffraction profile of the TiO_2 nanoparticles. Both anatase and rutile phase exist in the as-prepared TiO_2 nanoparticles. The strong diffraction peaks at 25° and 48°, corresponding to face (101) and (200), respectively, are solid evidence of TiO_2 NPs in its anatase phase. The strong peaks at 27°, 36°, and 55°, corresponding to face (110), (101), and (211), respectively, indicate the existence of the rutile phase of TiO_2 NPs. All peaks are in good agreement with the standard spectrum of anatase and rutile TiO_2 (JCPDS no. 84-1286 and 88-1175).

To impart the hybrid cell with higher power conversion efficiency than an individual cell, the sensitizers on the two photoanodes should have a complementary absorption spectrum for solar energy. Thus, the UV-Vis absorption spectra and

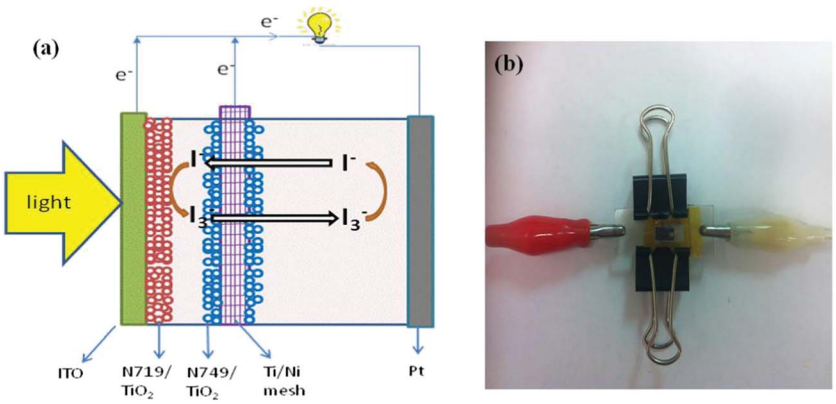

Fig. 1 (a) Schematic illustration of dye-sensitized solar cells with double-layered photoanodes. (b) Photo of the hybrid cell device.

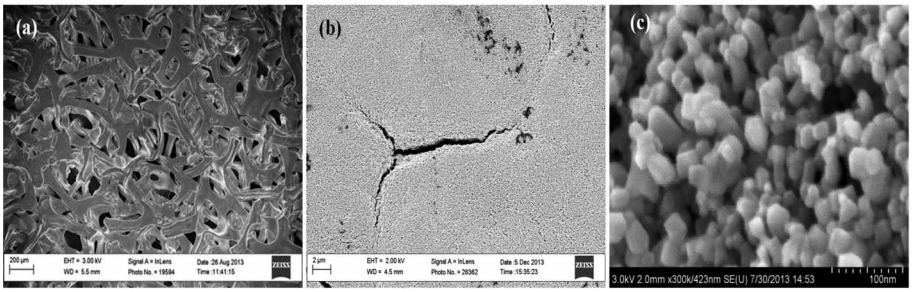

Fig. 2 SEM images of (a) the Ti/Ni mesh; (b) TiO_2 nanoparticles on the Ti/Ni mesh; (c) TiO_2 nanoparticles on ITO glasses.

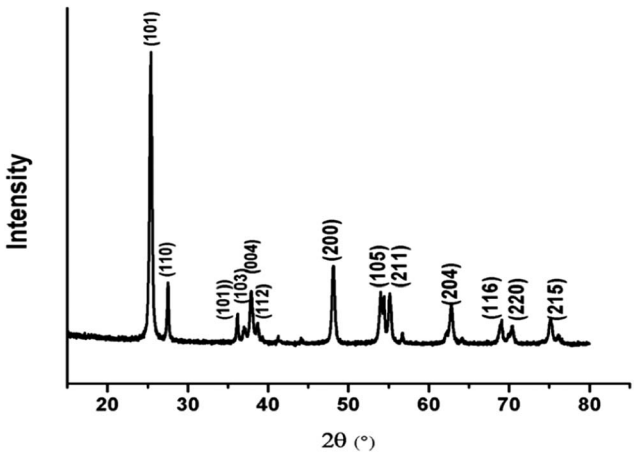

Fig. 3 X-ray diffraction patterns of TiO_2 nanoparticles.

IPCE spectra of N719 and N749 sensitized solar cells were measured, as shown in Fig. 4(a) and (b). UV-Vis spectra in Fig. 4(a) show that N719 sensitized solar cells have a strong absorption band in the range of 500–800 nm with a maximum peak at $\lambda = 556$ nm; N749 sensitized solar cells have two peaks in the range of 400–500 nm and 600–800 nm, with maximum peaks at $\lambda = 450$ nm and $\lambda = 647$ nm. In Fig. 4(b), the IPCE spectra of individual N719 and N749 show peaks in the similar positions as compared to UV-Vis spectra. Comparing the N749 IPCE spectra with N719 spectra, a stronger absorption was observed in the range of 600–800 nm. The IPCE of the hybrid cell indicates better absorption across the broad spectral range. These results suggest that the N719 sensitized TiO_2 absorbs solar energy in the shorter wavelength region firstly, and then the longer wavelength light is further captured by the N749 sensitized TiO_2 in the second photoanode. The two dyes used in this study nearly cover the whole panchromatic spectra in the range of visible light.

The photocurrent density–voltage (J–V) characteristics of the individual N719 sensitized solar cell on ITO glass (N719 cell), individual N749 sensitized solar cell on the Ti/Ni mesh (N749 cell) and the hybrid cell are compared in Fig. 5(a). Important parameters, including open-circuit voltage V_{oc}, short-circuit current density J_{sc}, fill factor FF, and power conversion efficiency η, are summarized in Table 1. The short-circuit current density (J_{sc}) at one sun illumination (standard illumination at AM1.5, or 1 kW m^{-2}) for the hybrid cell is 13.8 mA cm^{-2}, which is much higher than either of the single cell, *i.e.* 9.2 mA cm^{-2} for N719 cells and 8.84 mA cm^{-2} for N749 cells. The significant increase in J_{sc} reflects the parallel-connected nature of the hybrid cell and also substantiates the results of the UV-Vis and IPCE spectra, suggesting that the hybrid cell can capture a nearly panchromatic spectrum of the sun light. It is interesting to see that the V_{oc} of the hybrid cell is close to the average of single cells V_{oc} (*i.e.* $V_{oc\text{-hybrid}} \approx 1/2(V_{oc\text{-cell1}} + V_{oc\text{-cell2}})$). Lee *et al.*,[31] Miao *et al.*[32] and Nelles *et al.*[28] carried out similar experiments on multi-layered TiO_2 with different dyes but by other methods. The relationship between the V_{oc} of the whole

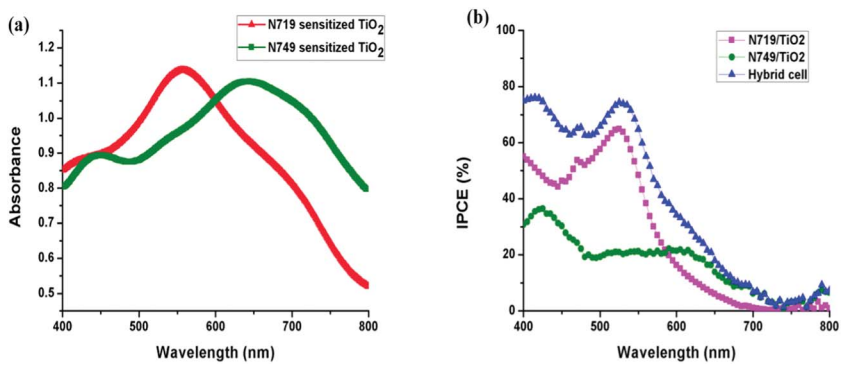

Fig. 4 (a) UV-Vis spectrum of the N719/TiO_2 film and the N749/TiO_2 film. (b) IPCE spectra of the N719-sensitized TiO_2 cell, N749-sensitized TiO_2 cell, and the hybrid cell.

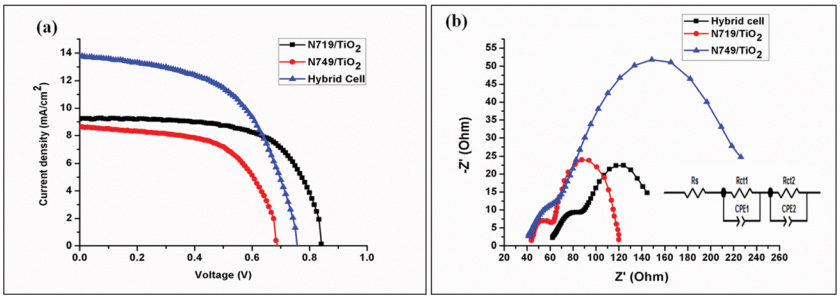

Fig. 5 (a) Photocurrent density–voltage (J–V) curves of the individual N719-sensitized TiO_2 cell (black line), the individual N749-sensitized TiO_2 cell (red line), and the hybrid cell (blue line). (b) Electrochemical impedance spectroscopy of the individual N719-sensitized TiO_2 cell (red line), the individual N749-sensitized TiO_2 cell (blue line), and the hybrid cell (black line). The equivalent circuit is inserted in the bottom right of the figure.

Table 1 Photovoltaic parameters of the hybrid cell and the individual N719 and N749 cells

	V_{oc} (V)	J_{sc} (mA cm^{-2})	FF	η (%)
N719 cell	0.84	9.2	0.66	5.2
N749 cell	0.69	8.64	0.61	3.5
Hybrid cell	0.76	13.8	0.56	6.6

cell and that of each single in their research agrees with the results in our experiments. The V_{oc} of a DSSC can be calculated by the following equation

$$V_{oc} = \frac{RT}{\beta F} \ln\left(\frac{AI}{n_0 k_b [I_3^-] + n_0 k_r [D^+]}\right),$$

where R is the molar gas constant, T is the temperature, F is the Faraday constant, β is the reaction order for I_3^- and electrons, A is the electrode area, I is the incident photon flux, n_0 is the concentration of accessible electronic states in the conduction band, and k_b and k_r are the kinetic constants of the backreaction of the injected electrons with triiodide and the recombination of these electrons with oxidized dyes (D^+), respectively. Since the loss term $n_0 k_r[D^+]$ can be neglected and $[I_3^-]$ can be considered as constant, V_{oc} depends logarithmically on $1/k_b$, ($k_b = \omega_{max}$,[33] where ω_{max} refers to the peak frequency of the second arc). From the results of electrochemical impedance spectroscopy (EIS) shown in Fig. 5(b), the peak frequency of the hybrid cell (ω_{max}) is 7.15 Hz, which is in the middle of those of single cells (*i.e.*, ω_{max} = 18.62 Hz for the N719 cell and ω_{max} = 4.98 Hz for the N749 cell). This explains why the V_{oc} values of hybrid cells are in between of those of N719 cells and N749 cells. Besides using Ti/Ni mesh as the substrate for the second photoanode, stainless steel mesh (SSM) was also tested. However, the V_{oc} of the SSM cell can only reach a value of 4.9 V, with a power conversion efficiency of 0.96%. The possible reason for the unsatisfactory performance of the SSM cell is that the SSM can be oxidized into Fe oxides at high temperature (around 500 °C) during sintering,[34–36] which greatly accelerates the back recombination of electrons at the TiO_2/dye/electrolyte interface. Thus, we adopted Ti/Ni mesh as the substrate for the bottom cell in our hybrid cell.

Notably a fill factor of 0.56 was measured for the hybrid cell, which is lower than that of the N719 cell and the N749 cell. The lower FF of the hybrid cell is probably due to the higher internal resistance compared to the single cell. The overall energy conversion efficiency for the hybrid cell is 6.6%, which is 21% (compared to the N719 cell) and 47% (compared to the N749 cell) higher than that of the single cell. The significant improvement in the efficiency of the hybrid cell proves that within the same dye-sensitized TiO_2 areas, the performance of the hybrid cell is much better than that of a single cell.

To study the kinetics of electron transport and recombination, electrochemical impedance spectroscopy (EIS) and an equivalent circuit were studied as shown in Fig. 5(b). The key parameters obtained from EIS measurements are listed in Table 2. Each EIS curve consists of two arcs. The first arc assigned in the high frequency scan region is related to the kinetics at the interface of Pt counter electrode/electrolyte. The diameter of the first arc is regarded as the resistance at the Pt surface (R_{ct1}), which is 20 Ω (N719 cell), 22 Ω (N749 cell), and 24 Ω (hybrid cell), respectively in our experiments. The similar R_{ct1} for the three cells agrees with the fact that the Pt counter electrodes are prepared under the same conditions. The second arc in the curve is assigned in the low frequency region, indicating the kinetics at the interface of TiO_2/dye/electrolyte. The diameter of the second arc is related to charge-transfer resistance for electron recombination (R_{ct2}), which is 56 Ω (N719 cell), 120 Ω (N749 cell), and 62 Ω (hybrid cell), respectively. Obviously, the charge combination resistance of the hybrid cell is in between the two individual cells. This is not surprising as the hybrid cells

Table 2 Parameters determined by the electrochemical impedance spectroscopy measurement[a]

	k_b (s^{-1})	τ_b (s)	R_s (Ω)	R_{ct1} (Ω)	R_{ct2} (Ω)
N719 cell	18.62	0.054	41	20	56
N749 cell	4.98	0.200	52	24	120
Hybrid cell	7.15	0.140	62	22	62

[a] k_b: effective rate constant for the recombination reaction, τ_b: effective electron lifetime for recombination, R_s: series resistance, R_{ct1}: charge transfer resistance related to the recombination of electrons, and R_{ct2}: resistance at the Pt surface.

combine the characteristics of individual N719 cell and N749 cells. Consequently the properties will be compromised. For the same principle, the effective recombination rate constant (k_b) and effective electron lifetime (τ_b) of the hybrid cells are also located in between of the single cells. R_s represents the series resistance of the circuit. It is reasonable to see that the series resistance of the hybrid cell is higher than either of the single cell.

Conclusions

In conclusion, uniquely structured dye-sensitized solar cells have been rationally designed and implemented by assembling two photoanodes (*i.e.*, ITO/TiO_2 and Ti/Ni mesh/TiO_2) and one Pt/ITO counter electrode in a single compartment. The power conversion efficiency of the hybrid cell (6.6%) is significantly higher than that of the single cell. The higher J_{sc} of the hybrid cell substantiates the signature of the parallel cell connection. The porous structure of the second photoanode enables the fabrication of the hybrid cell in a single compartment, by allowing the electrolyte to diffuse through the whole cell space. In sharp contrast to other hybrid/tandem cells which need the interconnecting layers, the two photoanodes were designed to be right next to each other, thereby eliminating the unnecessary loss of solar energy. As such, our study demonstrates an easy and scalable method to fabricate hybrid dye-sensitized solar cells with improved power conversion efficiency.

Acknowledgements

Xiaodan Zhang would like to thank the Institute of Paper Science and Technology at Georgia Tech for providing financial support.

Notes and references

1 B. Oregan and M. Gratzel, *Nature*, 1991, **353**, 737–740.
2 U. Bach, D. Lupo, P. Comte, J. E. Moser, F. Weissortel, J. Salbeck, H. Spreitzer and M. Gratzel, *Nature*, 1998, **395**, 583–585.
3 E. J. W. Crossland, N. Noel, V. Sivaram, T. Leijtens, J. A. Alexander-Webber and H. J. Snaith, *Nature*, 2013, **495**, 215–219.
4 A. Yella, H. W. Lee, H. N. Tsao, C. Y. Yi, A. K. Chandiran, M. K. Nazeeruddin, E. W. G. Diau, C. Y. Yeh, S. M. Zakeeruddin and M. Gratzel, *Science*, 2011, **334**, 629–634.
5 M. D. Ye, D. J. Zheng, M. Q. Lv, C. Chen, C. J. Lin and Z. Q. Lin, *Adv. Mater.*, 2013, **25**, 3039–3044.
6 M. D. Ye, H. Y. Liu, C. J. Lin and Z. Q. Lin, *Small*, 2013, **9**, 312–321.
7 Y. H. Jang, X. K. Xin, M. Byun, Y. J. Jang, Z. Q. Lin and D. H. Kim, *Nano Lett.*, 2012, **12**, 1742–1742.
8 J. Wang and Z. Q. Lin, *Chem. – Asian J.*, 2012, **7**, 2754–2762.
9 X. K. Xin, J. Wang, W. Han, M. D. Ye and Z. Q. Lin, *Nanoscale*, 2012, **4**, 964–969.
10 J. Wang and Z. Q. Lin, *Chem. Mater.*, 2010, **22**, 579–584.
11 M. D. Ye, X. K. Xin, C. J. Lin and Z. Q. Lin, *Nano Lett.*, 2011, **11**, 3214–3220.
12 X. K. Xin, M. He, W. Han, J. H. Jung and Z. Q. Lin, *Angew. Chem., Int. Ed.*, 2011, **50**, 11739–11742.
13 C. H. Siu, C. L. Ho, J. He, T. Chen, X. N. Cui, J. Z. Zhao and W. Y. Wong, *J. Organomet. Chem.*, 2013, **748**, 75–83.
14 N. Humphry-Baker, K. Driscoll, A. Rao, T. Torres, H. J. Snaith and R. H. Friend, *Nano Lett.*, 2012, **12**, 634–639.
15 J. Chang, C. P. Lee, D. Kumar, P. W. Chen, L. Y. Lin, K. R. J. Thomas and K. C. Ho, *J. Power Sources*, 2013, **240**, 779–785.
16 C. L. Lee, W. H. Lee and C. H. Yang, *J. Mater. Sci.*, 2013, **48**, 3448–3453.
17 G. D. Sharma, M. K. Panda, M. S. Roy, J. A. Mikroyannidis, E. Gad and A. G. Coutsolelos, *J. Renewable Sustainable Energy*, 2013, **5**, 023108.
18 N. C. Jeong, H. J. Son, C. Prasittichai, C. Y. Lee, R. A. Jensen, O. K. Farha and J. T. Hupp, *J. Am. Chem. Soc.*, 2012, **134**, 19820–19827.
19 C. Magne, M. Urien and T. Pauporte, *RSC Adv.*, 2013, **3**, 6315–6318.
20 V. Saxena, P. Veerender, A. K. Chauhan, P. Jha, D. K. Aswal and S. K. Gupta, *Appl. Phys. Lett.*, 2012, 100.
21 G. D. Sharma, S. P. Singh, R. Kurchania and R. J. Ball, *RSC Adv.*, 2013, **3**, 6036–6043.
22 H. Choi, S. Kim, S. O. Kang, J. J. Ko, M. S. Kang, J. N. Clifford, A. Forneli, E. Palomares, M. K. Nazeeruddin and M. Gratzel, *Angew. Chem., Int. Ed.*, 2008, **47**, 8259–8263.
23 C. M. Lan, H. P. Wu, T. Y. Pan, C. W. Chang, W. S. Chao, C. T. Chen, C. L. Wang, C. Y. Lin and E. W. G. Diau, *Energy Environ. Sci.*, 2012, **5**, 6460–6464.
24 K. M. Lee, Y. C. Hsu, M. Ikegami, T. Miyasaka, K. R. J. Thomas, J. T. Lin and K. C. Ho, *J. Power Sources*, 2011, **196**, 2416–2421.
25 F. Inakazu, Y. Noma, Y. Ogomi and S. Hayase, *Appl. Phys. Lett.*, 2008, **93**, 093304.
26 Z. M. Beiley and M. D. McGehee, *Energy Environ. Sci.*, 2012, **5**, 9173–9179.
27 W. S. Jeong, J. W. Lee, S. Jung, J. H. Yun and N. G. Park, *Sol. Energy Mater. Sol. Cells*, 2011, **95**, 3419–3423.
28 M. Durr, A. Bamedi, A. Yasuda and G. Nelles, *Appl. Phys. Lett.*, 2004, **84**, 3397–3399.
29 M. Murayama and T. Mori, *J. Phys. D: Appl. Phys.*, 2007, **40**, 1664–1668.
30 J. Usagawa, S. S. Pandey, S. Hayase, M. Kono and Y. Yamaguchi, *Appl. Phys. Express*, 2009, **2**, 062203.
31 K. Lee, S. W. Park, M. J. Ko, K. Kim and N. G. Park, *Nat. Mater.*, 2009, **8**, 665–671.
32 Q. Q. Miao, L. Q. Wu, J. N. Cui, M. D. Huang and T. L. Ma, *Adv. Mater.*, 2011, **23**, 2764–2768.
33 M. Adachi, M. Sakamoto, J. T. Jiu, Y. Ogata and S. Isoda, *J. Phys. Chem. B*, 2006, **110**, 13872–13880.
34 M. G. Kang, N. G. Park, K. S. Ryu, S. H. Chang and K. J. Kim, *Chem. Lett.*, 2005, **34**, 804–805.
35 L. J. Meng, M. X. Wu, Y. M. Wang, W. Guo, C. Y. Ma, T. L. Ma and R. Silva, *Appl. Surf. Sci.*, 2013, **275**, 222–226.
36 F. Y. Ouyang and W. L. Tai, *Appl. Surf. Sci.*, 2013, **276**, 563–570.